Since January 2020 Elsevier has created a COVID-19 resource centre with free information in English and Mandarin on the novel coronavirus COVID-19. The COVID-19 resource centre is hosted on Elsevier Connect, the company's public news and information website.

Colloids and Surfaces B: Biointerfaces 220 (2022) 112918

Contents lists available at ScienceDirect

Colloids and Surfaces B: Biointerfaces

journal homepage: www.elsevier.com/locate/colsurfb

Interaction of GC376, a SARS-COV-2 M^{PRO} inhibitor, with model lipid membranes

Mária Klacsová [a,*], Adriána Čelková [a], Alexander Búcsi [a], Juan Carlos Martínez [b], Daniela Uhríková [a]

[a] Department of Physical Chemistry of Drugs, Faculty of Pharmacy, Comenius University Bratislava, Odbojárov10, 832 32 Bratislava, Slovakia
[b] ALBA Synchrotron, Cerdanyola del Vallés 08290, Barcelona, Spain

ARTICLE INFO

Keywords:
GC376
SARS-CoV-2 antivirals
Lipid bilayer
Lateral pressure
Phase separation

ABSTRACT

Partitioning and effect of antiviral GC376, a potential SARS-CoV-2 inhibitor, on model lipid membranes was studied using dynamic light scattering (DLS), UV–VIS spectrometry, Excimer fluorescence, Differential scanning calorimetry (DSC) and Small- and Wide-angle X-ray scattering (SAXS/WAXS). Partition coefficient of GC376 between lipid and water phase was found to be low, reaching $K_P = 46.8 \pm 18.2$. Results suggest that GC376 partitions into lipid bilayers at the level of lipid head-groups, close to the polar/hydrophobic interface. Changes in structural and thermodynamic properties strongly depend on the GC376/lipid mole ratio. Already at lowest mole ratios GC376 induces increase of lateral pressures, mainly in the interfacial region of the bilayer. Hereby, the pre- and main-transition temperature of the lipid system increases, what is attributed to tighter packing of acyl chains induced by GC376. At GC376/DPPC $\geq$ 0.03 mol/mol we detected formation of domains with different GC376 content resulting in the lateral phase separation and changes in both, main transition temperature and enthalpy. The observed changes are attributed to the response of the system on the increased lateral stresses induced by partitioning of GC376. Obtained results are discussed in context of liposome-based drug delivery systems for GC376 and in context of indirect mechanism of virus replication inhibition.

1. Introduction

Pathogens such as coronaviruses (CoVs) are considered to be the major agents of emerging respiratory disease outbreaks. COVID-19 is the disease caused by acute respiratory syndrome coronavirus SARS-CoV-2 that emerged at the end of 2019 [36]. SARS-CoV-2 is a positive-sense single-stranded enveloped RNA virus that belongs to the β-lineage of the coronaviruses. CoVs genome with a size of 30 thousand bases encodes i.a. four vital structural proteins: nucleocapsid protein (N-protein), membrane protein (M-protein), envelope protein (E-protein), spike protein (S-protein), and two proteases: papain-like protease (PL^{pro}) and 3-chymotrypsin-like protease ($3CL^{pro}$), also called the main protease M^{pro}. M^{pro} is a key viral enzyme essential for the viral life cycle of CoVs, involved in the process of transcription and replication [6,15]. The structure of M^{pro} is highly conserved among coronaviruses. Therefore, it has been studied as a potential pharmacological target for specific antiviral drugs either using computer simulation techniques [10,56] as well as in experiments *in vitro* [1,22] and *in vivo* [23].

GC376, a dipeptide-based bisulfide adduct prodrug of aldehyde GC373, was discovered to strongly inhibit the M^{pro} of feline coronavirus FCoV [22]. Further studies showed its potency against a number of other coronaviruses including SARS-CoV-2 [16,51,52]. GC376 does not inhibit the unrelated influenza H1N1 virus, what suggests that its antiviral activity is specific [33]. The inhibition of M^{pro} by GC376 was determined within $IC_{50} = 0.03–0.16$ μmol.l^{-1}. The potent antiviral activity of GC376 against SARS-CoV-2 in the primary viral cytopathic effect assay reaches values of $EC_{50} = 2.19–3.37$ μmol.l^{-1} [16,33]. At the same time, the cytotoxicity of GC376 is low, with $CC_{50} > 100$ μmol.l^{-1}, thus is well-tolerated [33]. Recently, a dual mechanism of GC376 action by inhibiting both viral M^{pro} and host cathepsin L in Vero cells was supported by SARS-CoV-2 pseudovirus neutralization assay [15].

Solubility, as well as permeability and metabolic stability, affect oral bioavailability of a drug *in vivo* and contributes to accurate and reliable *in vitro* assays. The drug must pass across one or more phospholipid bilayers to reach the intracellular targets and elicit a response to their pharmacological action. The body's physiological processes like

* Corresponding author.
E-mail address: klacsova@fpharm.uniba.sk (M. Klacsová).

https://doi.org/10.1016/j.colsurfb.2022.112918
Received 31 July 2022; Received in revised form 26 September 2022; Accepted 9 October 2022
Available online 13 October 2022

opsonization or biotransformation issues are avoided by delivery systems for drug targeting. Targeted delivery systems seem to be necessary for drugs having low specificity, low therapeutic index, low absorption, short half-life, or a large volume of distribution. The use of stimuli-responsive lipid-based delivery systems take advantage of their sensitivity to both the endogenous stimuli, such as a change in temperature or glutathione concentration, and external stimuli, such as light or magnetic field [55]. Understanding the role of drug-lipid interactions on the pharmacokinetic properties of drugs is critical also in developing potent new antivirals [39]. According to Lipinski's rule [30], one of the parameters determining the bioavailability of a drug is its lipophilicity. GC376 has poor water solubility; critical micelle concentration of GC376 represents 96.7 mmol.l^{-1} [51].

Moreover, lipids play an essential role during viral infection involving membrane fusion of virus to host cell, viral internalization through receptor-mediated or lipid-microdomain-mediated endocytosis, viral replication and viral exocytosis. Coronaviruses bud from the endoplasmic reticulum/Golgi intermediate complex and exit via lysosomal secretion, thus the composition of the virion envelope significantly differs from plasma membrane. Lipidomic analysis of viral lipids extracted following infection of VeroE6 and A459 cells detected ~260 lipid species. The most abundant were phosphatidylcholines (PCs), phosphatidylethanolamines (PEs) and phosphatidylinositols (PIs) with fatty acid composition predominantly 16:0, 18:0, 18:1 [41]. Saud et al. [41] suggest the accessibility and importance of these lipids, which are unlikely to be affected by mutation of the virus, as potential target for antiviral approaches.

Here we present results that may help to complement lacking information on interactions of GC376 with lipid membranes. First, we used dynamic light scattering to elucidate the effect of GC376 on the size of unilamellar lipid vesicles (ULVs). Vesicle size may affect bioavailability and delivery to tissues outside of the vascular space. The partition coefficient K_P of GC376 between the water and the fluid lipid phase was determined using UV–VIS spectrophotometry. The lipid-water partition coefficient is a useful parameter in study of quantitative structure-activity relationships and in evaluating the permeability of drugs across the membrane. By definition, the partition coefficient does not offer any kind of topographical information about the drug localization in a membrane, which can be either adsorbed at the membrane surface or, in the case of a nonpolar species, intercalated within the hydrophobic part. We aimed to elucidate the information about GC376 localization within the membrane by monitoring the bilayer lateral pressure change using excimer fluorescence spectrometry. To study the effect of GC376 on the thermodynamic properties of model membranes in ULVs, differential scanning calorimetry (DSC) was used. The obtained thermodynamic parameters related to interactions of the drug with the lipid bilayer can be useful at the drug carrier designing when considering the drug bioavailability and stability of the drug-lipid suspensions. Finally, the structure of the lipid-GC376 system was investigated using small- and wide-angle X-ray scattering to get a detailed view about interaction of the antiviral with model lipid bilayer on molecular level.

As a model of fluid membrane in K_P, vesicle size and lateral pressure determination we used bilayers prepared from synthetic dioleoylphosphatidylcholine (DOPC), a lipid frequently used in liposomal-based drug-delivery systems [26,29,42]. In calorimetric and structural studies dipalmitoylphosphatidylcholine (DPPC) was used as a model of thermosensitive liposome [26,29]. DPPC-based liposomes display slower *in vivo* elimination rate [28] and less obvious Accelerated blood clearance phenomenon compared to DOPC-based liposomes [54].

2. Materials and methods

2.1. Chemicals

Synthetic lipids (DOPC, 1,2-dioleoyl-phosphatidylcholine; DPPC, 1,2-dipalmitoyl-phosphatidylcholine) were purchased from Avanti Polar Lipids (Alabaster, USA) and used without further purification. GC376 (sodium salt) was purchased from Biosynth Carbosynth (Bratislava, Slovakia). Excimer fluorescence probes (Pyr4PC, 1,2-bis-pyrenebutanoyl-phosphatidylcholine; Pyr10PC, 1,2-bispyrenedecanoyl-phosphatidylcholine) were purchased from Thermo Fisher Scientific (Massachusetts, USA). Chemical formulae of used chemicals are depicted on Fig S1. Organic solvents of spectral purity from Slavus (Bratislava, Slovak republic) were redistilled before use. 5 and 150 mmol.l^{-1} NaCl stock hydration media were prepared by dissolution of appropriate amount of sodium chloride (Lachema; Brno, Czech Republic) in MilliQ water (18.2 MΩ.cm, Millipore; Molsheim, France).

2.2. UV–VIS spectrometry

UV–VIS spectrometry was used for determination of partition coefficient of GC376 between lipid and water phase. GC376 was dispersed in NaCl hydration medium by a method of sequential hydration, described in [51], one day before the experiment. Briefly: Appropriate amount of GC376 was weighted into a conical vial and NaCl hydration medium was added in 0.5 μl increments at laboratory temperature. After each addition the mixture was vortexed and sonicated in a water bath for several times. This procedure was repeated until a clear, transparent solution of GC376 was obtained. Full dissolution of GC376, without presence of any aggregates, was proven by UV–VIS spectrometry; the absorption spectra of stock GC376 solution showed background close to zero, without any signs of scattering (Fig. 2). Multilamellar dispersion of DOPC was prepared on the day of experiment by dissolution of dry DOPC in appropriate amount of 150 mmol.l^{-1} NaCl hydration medium. Dispersion was homogenized by several thaw-freeze cycles and vigorous vortex mixing. Unilamellar DOPC vesicles (ULVs) were prepared by 51-times extrusion through 50 nm pores in carbohydrate filters (Nuclepore, USA) using Liposofast Basic Extruder (Avestin, Canada) at laboratory temperature [32]. A series of samples at concentrations of DOPC ULVs c_{DOPC} = 0.05–2.4 mmol.l^{-1} was prepared by dilution of corresponding amount of ULV dispersion with 150 mmol.l^{-1} NaCl hydration medium. Solution of GC376 was added into each sample, to reach final concentration of c_{GC376} = 1 mg.ml^{-1}. Sample concentration of GC376 was chosen as described in Results section. The system was incubated for 2 h with occasional vortexing at laboratory temperature prior to measurement. pH of prepared samples was within the range of pH = 6.6–6.8. Absorption spectra of prepared samples in a range of wavelengths λ = 190–820 nm were measured using a diode array spectrophotometer Agilent 8453 (Agilent Technologies, USA) in quartz cuvettes with optical path length of 1 cm. 150 mmol.l^{-1} NaCl hydration medium was used as a blank. Partition coefficient of GC376 between the lipid and water phase K_P was determined from obtained spectra as described in [12]: The scattering signal of ULVs was eliminated by numerical approximation of simplified Rayleigh's scattering function (Fig. S2) $A_\lambda = a.\lambda^b$, where A_λ is the absorbance at given wavelength λ and a, b are constants. The lipid/water partition coefficient of GC376 defined as

$$K_P = \frac{n_{GC376-DOPC} / \; V_{DOPC}}{n_{GC376-w} \; / \; V_w} \quad (1)$$

was determined by simultaneous fitting of $A_\lambda^{diff} = f(c_{DOPC})$ dependence for odd λ = 251–263 nm with a function

$$A_\lambda^{diff} = \frac{l.n_{GC376}(\varepsilon_{GC376-w}V_w + \varepsilon_{GC376-DOPC}K_P V_{DOPC})}{K_P V_{DOPC} + V_w} \quad (2)$$

where A_λ^{diff} is the absorbance read from the difference spectra (i.e. after subtraction of scattering function); c_{DOPC} is sample concentration of lipid; n_{GC376} is total number of moles of GC376 in a given volume, which equals the sum of number of moles of GC376 in water and lipid phase, i.e. $n_{GC376} = n_{GC376-w} + n_{GC376-DOPC}$; $\varepsilon_{GC376-w}$ and $\varepsilon_{GC376-DOPC}$ are molar absorption coefficient of GC376 in water and in lipid phase, respectively; V_w and V_{DOPC} are molar volumes of water and lipid. Molar

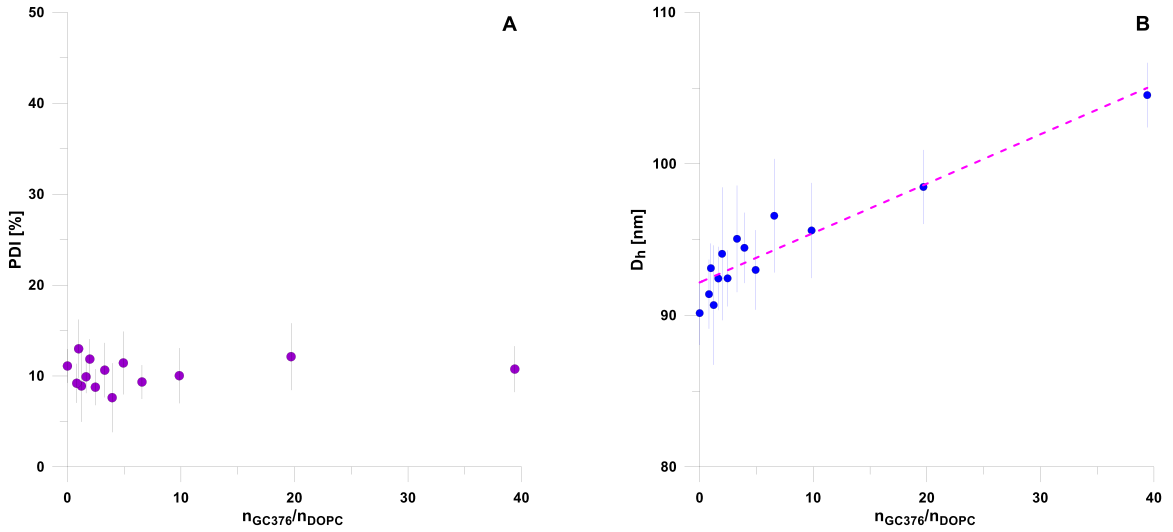

Fig. 1. Polydispersity index (Panel A) and hydrodynamic diameter D_h (Panel B) of DOPC+GC376 vesicles in NaCl hydration medium as a function of GC376/DOPC mole ratio. Error bars represent the standard deviation of three measurements; dashed line is the error weighted best linear fit of the experimental points.

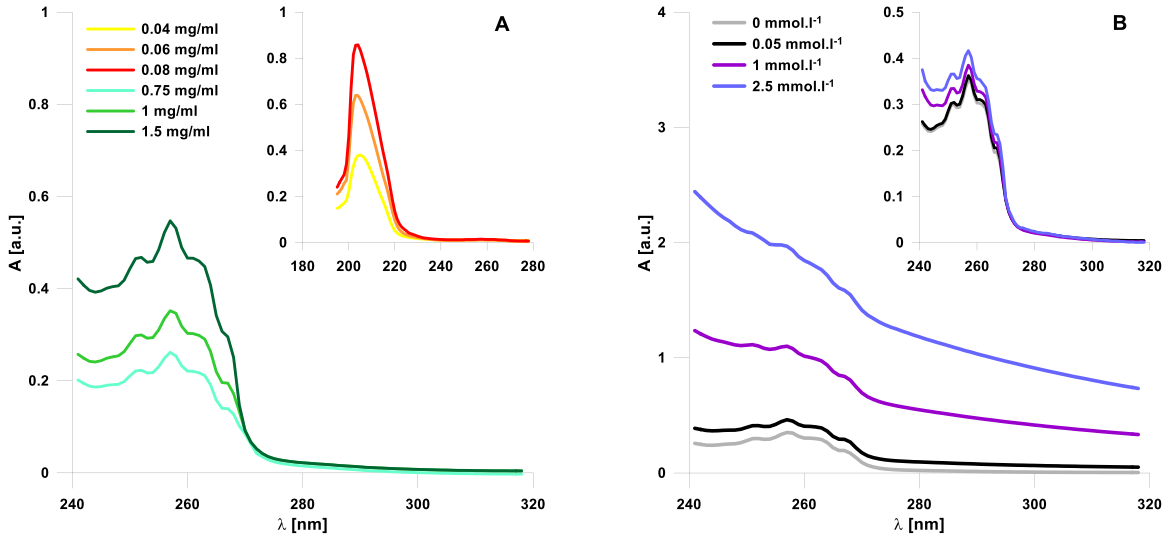

Fig. 2. Panel A: UV–VIS absorption spectra of GC376 in NaCl hydration medium without ULVs at designated GC376 concentration. Panel B: Selected UV–VIS absorption spectra obtained for GC376 after incubation with DOPC ULVs of designated concentration in NaCl hydration medium before (main graph) and after (inset) subtraction of Rayleigh's scattering on ULVs.

volume of the water phase can be expressed as $V_w = 1\text{-}V_{DOPC}$. Molar volume of the lipid phase is defined as $V_{DOPC} = n_{DOPC}$. M_{DOPC}/ρ_{DOPC}, where n_{DOPC} is number of moles of lipid; M_{DOPC} is molar mass of lipid and ρ_{DOPC} is density of lipid. For DOPC a value of $\rho_{DOPC} = 1.0096013$ g. ml^{-1} [45,47] was used.

2.3. Dynamic light scattering (DLS)

Method of DLS was used to check the size and polydispersity of ULVs in samples prepared for determination of K_P (Section 2.2). Side scattering (90°) was collected using Litesizer 500 (Anton Paar, Austria) over 60 runs; duration of a single run was 10 s. Measurement was performed in a disposable cuvette at 25 °C with equilibration time of 60 s. Sample temperature was controlled through a Peltier to within ± 0.1 °C. Three independent measurements were performed for each sample. Experimental data were evaluated by the DLS analysis software, where the hydrodynamic diameter D_h is calculated using the Stokes-Einstein equation

$$D_h = \frac{k_B T}{3\pi\eta D_t} \quad (3)$$

where D_t is translational diffusion coefficient, k_B is Boltzmann's constant, T is thermodynamic temperature and η is dynamic viscosity.

2.4. Excimer fluorescence

For detection of lateral pressure change across the DOPC bilayer in presence of GC376 the method of excimer fluorescence was used [7]. Two sets of samples were prepared in order to monitor lateral pressure change in different depths of the bilayer, depending on the position of the pyrene moieties in bispyrenyl fluorescent probes (Pyr*n*PC, $n = 4, 10$) [43]. DOPC, Pyr4PC and Pyr10PC, respectively, were dissolved at known concentrations in an organic solvent (methanol:chloroform = 1:1 vol/vol), GC376 was dissolved in ethanol. Required volumes of DOPC, GC376 and Pyr*n*PC were mixed together. The organic solvent was evaporated under a stream of nitrogen gas and its rests removed under

vacuum. Dried samples were hydrated by addition of 150 mmol.l^{-1} NaCl hydration medium and homogenized by vigorous vortex mixing. Prepared dispersions were sonicated during several seconds and stored one day in a refrigerator for equilibration. Prior to measurement, samples were vortexed and mildly sonicated again. The final concentration of DOPC+GC376 was 0.1 mmol.l^{-1} and the Pyr*n*PC:(DOPC+GC376) mole ratio was 1:1500. Fluorescence measurements were performed using a quartz cuvette with optical path length of 1 cm in a fluorimeter FluoroMax-4 (HORIBA Jobin Yvon, France). The emission spectrum was collected after excitation at $\lambda_{ex} = 345$ nm in the region of $\lambda_{em} = 360–650$ nm with the increment of 0.5 nm and integration time for each wavelength 0.1 s. The excitation and emission bandwidths were 5 and 2 nm, respectively. Fluctuation of fluorescence intensity was monitored at $\lambda_{ex} = 345$ nm and fixed emission, $\lambda_{em} = 376$ nm (pyrene monomer emission) and 481 nm (pyrene excimer emission), respectively, during 120 s (Fig. S5). Measurements were performed at 25, 30, 37 and 42 °C; temperature of the sample was regulated to within ± 0.01 °C by a Peltier thermocouple drive. Correction for spectral response was applied, i.e. the value of S1c/R1c was monitored, where S1c and R1c denote the signal detector and reference (lamp) detector corrections, respectively, for wavelength- and time-dependent response. The ratio of the excimer-to-monomer intensities provide a measure of lateral pressure η within the bilayer plane [44]:

$$\eta = \frac{I^E}{I^M} \tag{4}$$

where the I^M and I^E denote the average intensity of the monomer and excimer emission detected at 376 and 481 nm, respectively, during time-based measurement.

2.5. Differential scanning calorimetry (DSC)

Effect of GC376 on phase transition temperatures and thermodynamic parameters of model DPPC membranes was determined using a Nano DSC calorimeter (TA Instruments, USA). Samples were prepared as follows: DPPC and GC376 were dissolved at known concentrations in methanol and ethanol, respectively. Required volumes of DPPC and GC376 solutions were mixed together, the organic solvents were removed under a stream of nitrogen gas and rests removed under vacuum. Dry films were hydrated using 5 mmol.l^{-1} NaCl hydration medium, to obtain lipid dispersions of 5 mg.ml^{-1} concentration. Low concentration of NaCl, compared to other techniques, was used to prevent deformation of calorimetric traces observed at higher ionic strengths [4]. Samples were homogenized by vigorous vortexing and freezing-thawing cycles and stored in a refrigerator overnight. Thereafter, samples were diluted in a 1:4 vol/vol ratio using 5 mmol.l^{-1} NaCl hydration medium. To prevent sedimentation of liposomes during the measurement, dispersions were extruded through 100 nm pore-size filter (Nuclepore, USA) in a LiposoFast LF-50 extruder (Avestin, Canada) at 60 °C. Prior to measurement ULV samples were degassed using a Degassing station (TA Instruments, USA) for 15 min at temperature 4 °C and pressure 230 Torr.

The DSC reference cell was loaded with 5 mmol.l^{-1} NaCl hydration medium. No pressure was applied during the measurement. Three heating-cooling cycles were measured for each sample in a temperature range 5–60 °C with a heating rate of 1 °C.min^{-1} and a pre-equilibrium halt of 1000 s. The third heating scan of each sample was chosen for evaluation using the OriginPro program (OriginLab Corp., USA). In the excess heat capacity thermograms $C_p = f(t)$ first a linear baseline, obtained by extrapolation of pre- and post-transition output, was subtracted. Experimental data were then fitted by an asymmetric Pearson function

$$C_p = \frac{C_p^{max}}{\left[1 + 4\left(\frac{t - t^{max}}{\Delta t_1}\right)^2 \left(2^{\frac{1}{\Delta t_2}} - 1\right)\right]^{\Delta t_2}} \tag{5}$$

where C_p^{max} is heat capacity maximum; t^{max} is temperature corresponding to C_p^{max}, corresponding thus to phase transition temperature; Δt_1 and Δt_2 are half-widths of the peak. The change in enthalpy ΔH was calculated by standard integration procedures [13].

2.6. X-ray scattering

In order to investigate the structure of DPPC+GC376 complexes small- and wide-angle X-ray diffraction (SAXS/WAXS) experiments were performed on beamline BL11-NCD-SWEET at the ALBA synchrotron (Barcelona, Spain). Samples were prepared in advance following the procedure described in Section 2.5. Dry lipid film was hydrated by 150 mmol.l^{-1} NaCl hydration medium to obtain 16 mg.ml^{-1} dispersions. Samples were homogenized by vigorous vortexing and freezing-thawing cycles. After that, samples were centrifuged at 13,000 rpm for 2 min using Minispin centrifuge (Eppendorf, Germany). The sediment was transferred into thin-walled quartz capillaries (Hilgenberg, Germany) with a diameter of 1.5 mm and closed with a plasticine. Measurements were performed using a monochromatic radiation of wavelength 0.12 nm. The capillary samples were placed vertically in a Linkam stage, which provided the temperature control. Samples were measured at 20 and 60 °C. The heating program was as follows: 3 min incubation of a sample at respective temperature, 1 s exposure, heating to next temperature with a ramp of 1 °C.min^{-1}. Selected samples were measured repeatedly to exclude possible radiation damage due to selected exposure time. SAXS data were detected on a Pilatus 1 M detector calibrated using AgBh [14]. WAXS data were detected on a LX255HS Rayonix detector calibrated using Cr_2O_3 (certificate SRM 674b, NIST, USA). The 2D scattering patterns were azimuthally integrated into 1D data using the pyFAI python library [21]. Intensity profiles were normalized to the intensity of the incident beam. The diffraction peaks were fitted with Lorentzian functions and linear background [37]. The bilayer repeat distance d of the lamellar phase was calculated as

$$d = 2\pi/q \tag{6}$$

where q is the position of the first lamellar SAXS peak.

3. Results

3.1. Vesicle size

As a model lipid system ULVs prepared from DOPC were used, due to the fluid phase of this lipid at laboratory temperature [35]. Gel phase lipid would provide more distorted data, as a consequence of the higher refractive index of bilayers in comparison to the fluid phase [40]. For all measured samples the correlation function showed a smooth single exponential decay suggesting a relatively monodisperse system of small-sized vesicles and absence of aggregates (Fig. S2A). The vesicle size distribution proved the uniformity of vesicles in all samples (Fig. S2B). Broadness of the vesicle size distribution is given by a polydispersity index (PDI) value.

Fig. 1 shows PDI as a function of GC376/DOPC mole ratio. Polydispersity of vesicle size was not changing with the GC376/DOPC mole ratio; the mean polydispersity index (PDI) reached a value of 10.3 ± 2.7%, what indicates that all of the measured ULVs have almost the same size [2]. The hydrodynamic diameter of DOPC+GC376 vesicles showed an increasing dependence on GC376/DOPC mole ratio (Fig. 1B), from initial 90.2 ± 2.1 nm obtained for pure DOPC ULVs up to 104.5 ± 2.1 nm at $n_{GC376}/n_{DOPC} = 39.4$ mol/mol. Noticeably, these values

does not correspond to absolute vesicle size. Since DLS measures the average hydrodynamic diameter of the particles, the mean diameter measurements are shifted towards larger values. Moreover, synthetic lipid vesicle systems exhibit a pronounced hydration shell of 10–16 nm [49], which is also included in the vesicle size values. Anyway, the observed increase in D_h with GC376 concentration indicates that GC376 molecules interact with DOPC bilayers. To quantify this interaction partition coefficient of GC376 between the water and lipid phase has been determined.

3.2. Partition coefficient

First, we measured the absorption spectra of GC376 in NaCl hydration medium without ULVs. At concentrations below 0.1 mg.ml^{-1} GC376 (Fig. 2A inset) a single well-resolved absorption peak was detected with a maximum at $\lambda = 206$ nm. This peak lies in the region of absorption of lipid molecules [12], thus it is not suitable for determination of K_P. By a tenfold increase of GC376 concentration, we succeeded to obtain a group of absorption bands, typical for conjugated double bonds, with a maximum at $\lambda = 257$ nm (Fig. 2A). From the value of absorbance at 257 nm a molar absorption coefficient of GC376, $\varepsilon_{257} = 182.48$ cm^2.mmol^{-1}, was determined.

Consecutive increase of GC376 concentration led to proportional increase in absorption, however the resolution of the bands improved only slightly. Position of the maxima did not change with concentration. According to DLS results, the interaction with GC376 increases the size of ULVs, what in turn affects the light scattering on ULVs. Concomitantly, a significant increase in absorption values is expected. For further experiments a total sample concentration of 1 mg.ml^{-1} GC376 was chosen, in order to obtain well-resolved spectra at measurable absorbance values.

Typical absorption spectra obtained for GC376 after incubation with DOPC ULVs are displayed on Fig. 2B. As supposed, with increasing DOPC concentration an increase in absorption values and resultant deformation of GC376 absorption spectrum was detected. The unwished background was eliminated by fitting (Fig. S3). Resulting difference spectra (Fig. 2B inset) showed background close to A = 0, what indicates that the scattering was satisfactorily eliminated.

K_P was determined from changes in GC376 absorbance, caused by binding of GC376 to ULVs, by simultaneous fitting of $A_\lambda^{diff} = f(c_{DOPC})$ dependence for odd $\lambda = 251$–263 nm, as described in Section 2.2. A nonlinear least squares method was used to approximate each dependence by a theoretical function (Eq.2). Fitted experimental dependences are summarized on Fig. S4. High values of correlation coefficient of approximations ($r^2 = 0.994$–0.998) give the evidence that used theoretical function satisfactorily fit all experimental points and may thus be used for determination of K_P. Value of GC376 partition coefficient determined in the DOPC/water system represents $K_P = 46.8 \pm 18.2$.

3.3. Lateral pressure

Lateral pressures in the acyl chain region near the hydrophilic/hydrophobic interface and near the bilayer core were monitored using Pyr4PC and Pyr10PC fluorescence probes, respectively. Fig. 3A shows typical emission spectra obtained for pure DOPC bilayers in 150 mmol. l^{-1} hydration medium at 25 °C. Two intensive monomer emission peaks, at $\lambda^M = 376$ and 396 nm, corresponding to pyrene vibronic bands I and IV, and a broad unstructured excited state dimer (excimer) emission band, with a maximum at $\lambda^E = 481$ nm, that involves interaction of two periplanar pyrene groups, can be resolved [3]. Spectra are normalized to the intensity of the first monomer maxima, $I^M_{Norm}(376) = 100$. Thus, by simple comparison of excimer intensities we can deduce, that lateral pressure is lower in the hydrophobic interior of the bilayer than near the hydrophilic/hydrophobic interface, as a consequence of $I^E_{Norm}(Pyr10PC) < I^E_{Norm}(Pyr4PC)$. To quantify this difference, the ratio of excimer-to-monomer emission intensities (Eq. 4) was calculated. This ratio provides the measure of the rate of excimer formation, which is determined by the frequency of collisions between pyrene moieties, and hence can be related to parameter describing the lateral pressure η within the bilayer plane. Increasing the pressure increases the average number of collisions per second and so enhances the probability of excimer formation [7]. For pure DOPC values of $\eta_{Pyr4PC} = 1.135 \pm 0.030$ and $\eta_{Pyr10PC} = 0.558 \pm 0.011$ were obtained by respective fluorescence probes.

The dependence of lateral pressure on GC376/DOPC mole ratio as detected by the Pyr4PC and Pyr10PC fluorescence probes at 25 °C is shown on Fig. 3B. With increasing amount of GC376 an increase of lateral pressure is observed up to 0.05 mol/mol. Over 0.05 mol/mol the value of lateral pressure changes only within the experimental error. This trend was observed for both fluorescence probes used. However, the lateral pressure increase detected by Pyr4PC is, compared to the increase detected by Pyr10PC, three times higher.

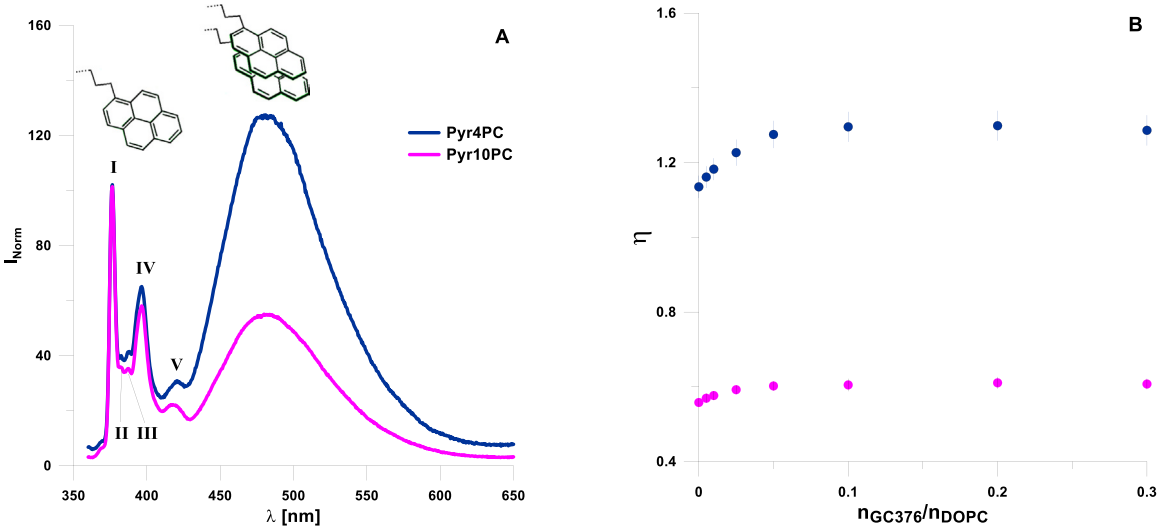

Fig. 3. Panel A: Normalized fluorescence emission spectra of Pyr4PC and Pyr10PC in DOPC bilayers at 25 °C with designated vibronic bands of pyrene monomer (I-V). Schemes represent the pyrenyl fragments of the lipid-based probes in the monomer and dimer organization at corresponding wavelength regions. Panel B: Lateral pressure as a function of GC376/DOPC mole ratio detected by Pyr4PC and Pyr10PC fluorescence probes, respectively, at 25 °C. Error bars denote the standard deviation determined from the time-based measurements of fluorescence intensities.

With increasing temperature, the increase of lateral pressure as a function of n_{GC376}/n_{DOPC} becomes more significant, both for Pyr4PC and for Pyr10PC, respectively. The dependence of lateral pressure on the temperature for selected GC376/DOPC mole ratios as obtained by Pyr4PC and Pyr10PC is shown on Fig. S6. For a given mole ratio, the lateral pressure increases linearly within the studied temperature range. In case of pure DOPC the lateral pressure increases with temperature more steeply close to the hydrophilic/hydrophobic interface than in the bilayer hydrophobic core, as deduced from the comparison of the slopes, $a_{Pyr4PC} = 0.053 > 0.028 = a_{Pyr10PC}$. Observed temperature induced increase of lateral pressure is in accord with previously reported data, however the absolute value of the increase differs to $a = 0.016$[1] obtained with Pyr10PC [50] and $a = 0.054$[1] obtained with Pyr14PC [25] in DOPC bilayers. With increasing GC376/DOPC mole ratio further increase of the slope is observed for Pyr4PC, while for Pyr10PC the slope changes with GC376/DOPC mole ratio only within the experimental error.

3.4. Thermodynamic parameters

For DPPC liposomes, we observe two phase transitions within the studied temperature range (Fig. 4): a pre-transition between the highly organized $L_{\beta'}$ gel phase and the rippled P_β gel phase, and a main transition between the P_β phase and the disordered liquid-crystalline L_α phase. The slight asymmetry of the main transition peak on the left side is typical for DPPC liposomes extruded through filters with small pore-size [9]. With increasing amount of GC376 the intensity of the pre-transition systematically decreases and finally, at 0.03 mol/mol the pre-transition disappears. The main transition displays broadening upon

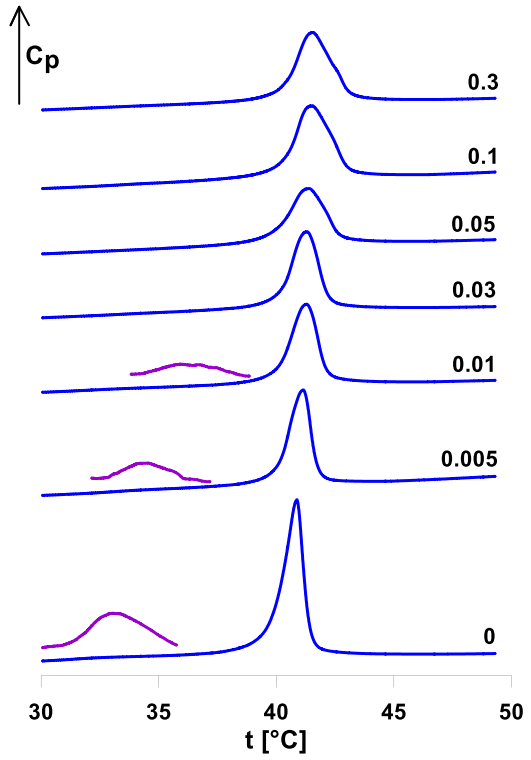

Fig. 4. Temperature dependence of the heat capacity C_p obtained upon third heating of the DPPC+GC376 system at different GC376/DPPC mole ratios. The insets represent 60 times enlarged areas of the pre-transition peak.

[1] Value of slope obtained by fitting of digitalized data from the related articles.

increasing GC376/DPPC mole ratio. Up to 0.01 mol/mol endotherms were fitted with a single-Pearson function, reaching correlation coefficient of fitting $r^2 > 0.999$. The endotherm measured at 0.03 mol/mol was at the first attempt fitted with a single-Pearson function; the correlation coefficient of this fit was $r^2 = 0.992$. However, a double-Pearson fit yielded a better correlation with $r^2 = 0.999$. Thus, we assume, that already at 0.03 mol/mol a splitting of the endotherm is present. At higher GC376/DPPC mole ratios the splitting was more obvious, these endotherms could be satisfactorily fitted with two Pearson functions (Fig. S7).

Phase transition temperatures and transition enthalpies as determined from the heating endotherms are shown on Fig. 5 as a function of GC376/DPPC mole ratio. For the pre-transition of pure DPPC these values represent $t_p = 33.1$ °C and $\Delta H_p = 3.76$ kJ.mol^{-1}, for the main transition $t_m = 40.8$ °C and $\Delta H_m = 38.22$ kJ.mol^{-1} were obtained. These results fit well within the range of values determined previously for DPPC in DSC studies [38,46].

With increasing amount of GC376 the pre-transition temperature significantly increases, whereas the enthalpy decreases, reaching $t_p = 36.0$ °C and $\Delta H_p = 0.69$ kJ.mol^{-1}, respectively, at 0.01 mol/mol. The main transition shows in this concentration range similar tendency, both for transition temperature t_m as well as for transition enthalpy ΔH_m. But, starting at 0.03 mol/mol the increase of t_m and the decrease of ΔH_m becomes less steep and stabilizes at values of ~ 41.3 °C and ~ 5.5 kJ.mol^{-1}, respectively. The flattening of the dependences is accompanied with the appearance of a new phase. In the following text, we will refer to the original phase as the L phase and the new phase as the L_n phase. Main transition temperature of the L_n phase is systematically higher, compared to the L phase. Hereby, the melting enthalpy of the L_n phase exceeds the enthalpy of the L phase and increases with the amount of GC376.

3.5. Structural parameters

Based on DSC results, SAXS/WAXS experiments for DPPC and DPPC+GC376 complexes were performed at 20 and 60 °C, in order to investigate structural changes in the gel and liquid-crystalline phase, respectively. Typical SAXS and WAXS patterns obtained for the studied systems are displayed on Fig. 6. DPPC forms in excess water lamellar phase with equidistantly stacked bilayers separated by aqueous layers. Consistently, two equidistant peaks were detected in the SAXS region at both temperatures. In the WAXS region two peaks can be distinguished at 20 °C (Panel A), a narrow (20) peak at q ~ 14.83 nm^{-1} and a broad (11) peak at q ~ 15.27 nm^{-1}, which are characteristic for the $L_{\beta'}$ gel phase with chains packed in a distorted hexagonal sublattice and tilted towards the nearest neighbours [34]. At 60 °C (Panel B) a wide diffuse scattering was detected in the WAXS region. Such patterns are typical for the lamellar fluid L_α phase with conformationally disordered hydrocarbon chains due to increased *trans-gauche* isomerization.

The addition of GC376 has a significant effect on SAXS/WAXS patterns predominantly in the gel phase (20 °C, Fig. 6A). Starting at GC376/DPPC = 0.05 mol/mol the SAXS peaks display visible broadening. Consequently, each peak of $L_{\beta'}$ lamellar phase was fitted as a superposition of two Lorentzian functions. The WAXS patterns show upon increasing amount of GC376 a systematic decrease in the intensity and shift in the position of the (20) peak towards higher q-values. At the same time, the intensity and the position of the (11) peak does not change significantly. In the fluid phase (60 °C, Fig. 6B) all SAXS patterns could be satisfactorily fitted with a single Lorentzian function. A significant change in the peak's maximum position accompanied with a decrease in their intensities is observed at 0.05 mol/mol. The WAXS region shows at 60 °C a diffuse scattering at all GC376/DPPC mole ratios studied.

The repeat distance d, defined as the thickness of the lipid bilayer (d_L) plus the water layer (d_W) separating the bilayers, was derived from the position of first peak (01) maximum according to Eq. 6. DPPC at

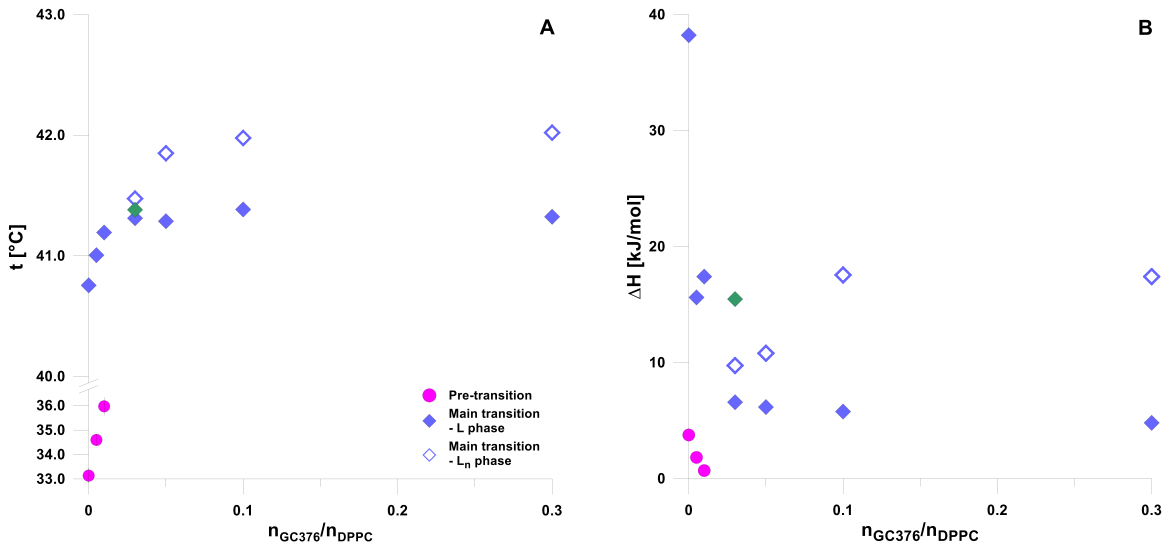

Fig. 5. Pre-transition and main phase transition temperature t (Panel A) and change in transition enthalpy ΔH (Panel B) as a function of GC376/DPPC mole ratio. Error bars denote the error of fitting. Where not signed, errors are within the symbol size. Green diamonds represent, for comparison, the t_m and ΔH_m values obtained for the 0.03 mol/mol using a single-Pearson function fit.

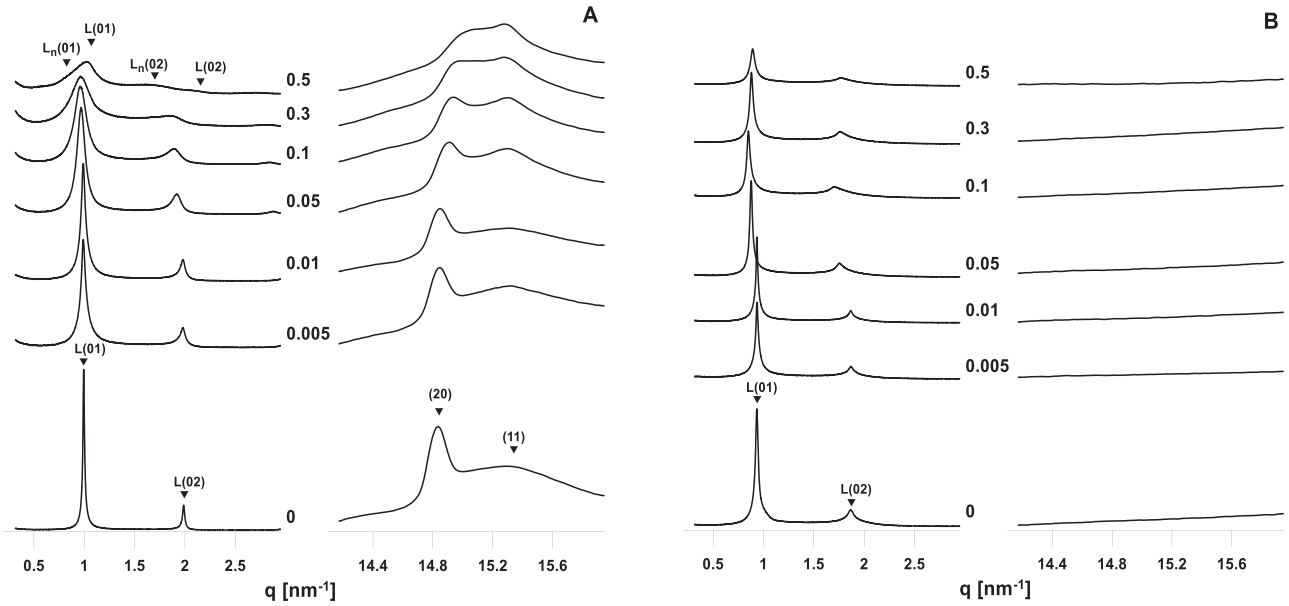

Fig. 6. SAXS and WAXS patterns obtained for designated GC376/DPPC mole ratios at 20 °C (Panel A) and 60 °C (Panel B). L and L_n, with respective Miller indices, denote peaks corresponding to the original and new lamellar phase, respectively.

20 °C shows a repeat distance of d = 6.31 ± 0.01 nm, which well agrees with literature [37,45,47]. On heating an increase of repeat distance is observed, reaching d = 6.71 ± 0.01 nm at 60 °C. Although the bilayer thickness decreases with increasing temperature, a simultaneous increase in water layer thickness overwhelms this change and contributes to overall increase in repeat distance [37]. Upon addition of GC376 the bilayer repeat distance increases up to 0.1 mol/mol and then decreases back, both at 20 °C as well as at 60 °C (Fig. 7). At the same time, repeat distance of the L_n phase, detected at 20 °C, significantly increases with GC376 concentration, reaching d = 7.50 ± 0.03 nm at 0.5 mol/mol.

4. Discussion

Partition coefficient is an important parameter in pharmacological and toxicological studies to determine the effective concentrations and kinetic behaviour of a drug in biological systems. Theoretically as well as experimentally most frequently used is the partition coefficient between *n*-octanol and water (K_{OW}). However, partition coefficient between phospholipid and water (K_P) is more relevant for the drug, modelling its pharmacokinetic behaviour in biological systems. The correlation between the K_{OW} and K_P is also not so straightforward, thus K_{OW} should be used cautiously [48]. Vaes et al. [48] derived an equation to calculate phospholipid/water partition coefficient from the estimated K_{OW} for polar compounds:

$$logK_P = 0.904 \times logK_{OW} + 0.515 \quad (7)$$

Using an estimated $\log K_{OW} = -0.68$ value for GC376 [11] the equation gives a value of $K_P = 0.8$, which is much lower than $K_P = 46.8 \pm 18.2$ that we have determined experimentally. This result further underlines the necessity of experimental determination of phospholipid/water partition coefficients. The main difference between the two values (K_P and K_{OW}) might result from the sharp interface between the

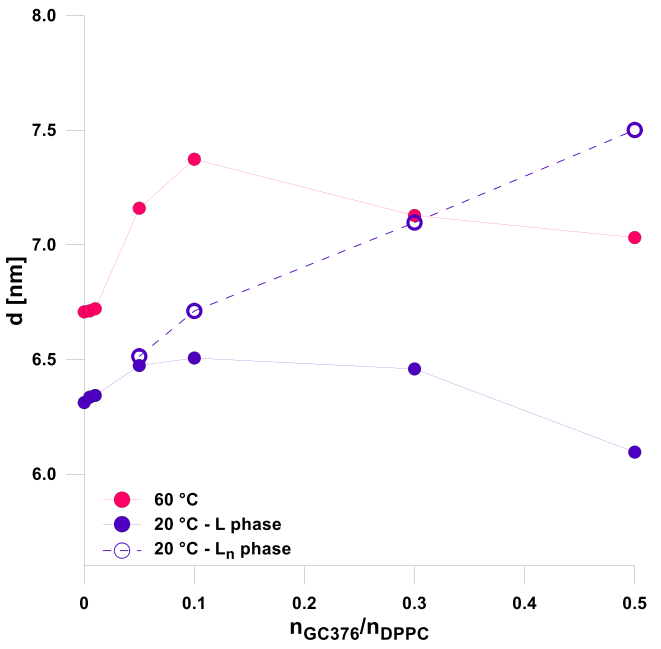

Fig. 7. Repeat distance d as a function of GC376/DPPC mole ratio at 20 and 60 °C. Lines connecting the symbols are meant to guide the eye. Errors are within the symbol size.

polar and hydrophobic region assumed for the *n*-octanol/water system. This is in contrast to the phospholipid/water system, where the transition between the two regions is not exactly defined and molecules of water penetrate rather deeply and interact with fragments of phospholipid's headgroup (as illustrated by e.g. Kučerka et al. [24]). The difference in K_P and K_{OW} should not be accounted to differences in phase state of the two systems, since partitioning into a fluid lipid bilayer was followed.

Value of K_P obtained suggests that the study of non-specific binding of GC376 to lipid bilayers is pertinent. The non-specific interaction might possibly play a role in indirect mechanism of GC376 antiviral action. Several studies have supported the evidence that lipid-binding domains in virus proteins are essential for virus replication [8]. The interaction of GC376 with Cov's lipid envelope, resulting in a change of structural and physicochemical properties of the lipid bilayer (as discussed later in this section), might affect the function of embedded proteins. Such implication was previously suggested for changes in lateral pressure [5], bilayer thickness [18] and phase transition of annular lipids [27].

Partition coefficient does not offer, in principle, any kind of topographical information about the drug localization in a membrane, which can be either adsorbed at the membrane surface or intercalated deeper into the bilayer. However, the relatively low value of K_P suggests that the GC376 molecule should be localized close to the polar/hydrophobic interface of the bilayer and interact preferably with the polar headgroup of the lipid molecule. This allows to assume that process of permeation of GC376 across the membrane will be very slow, what confirms the necessity of formulation of a suitable drug carrier. Based on the polar nature of GC376 molecule, it's delivery within the water core of a liposomal drug formulation would be assumed. Observed partitioning of GC376 into the lipid bilayer might affect the amount of released drug from liposomes *in vivo*. At the same time, the size and polydispersity of liposomes are affected by partitioning of GC376 only slightly (Fig. 1), thus the delivery and availability of the drug at site of action should not be affected by these parameters.

Assumption of localization of GC376 molecule close to the polar/hydrophobic interface of the bilayer is in line with observed changes in lateral pressure induced by GC376. In a native membrane the pressure at the polar/hydrophobic interface is strongly negative because of attractive forces between phospholipids glycerol groups, which are intended to limit the contact between water and hydrocarbon interior of the membrane. This is resisted in the chain region where is a strong positive pressure due to thermally driven collisions between acyl chains. In the head-group region of phosphatidylcholines again positive contributions to the lateral pressure are present, which arise from steric, hydrational and charge effects. Hereby, the overall lateral pressure across the membrane is zero [44]. We found that addition of GC376 induces three times higher increase of lateral pressure near the polar/hydrophobic interface than in the hydrophobic interior of the bilayer. It further suggests that the bulky molecule of GC376 is localized in the region of lipid head-groups, close to the polar/hydrophobic interface.

To gain further insight into the effect of GC376 on lipid bilayer and to quantify it, we performed thermodynamic and structural studies on DPPC+GC376 system. DSC results show that up to GC376/DPPC = 0.01 mol/mol the pre-transition temperature t_p of DPPC from gel $L_{\beta'}$ to rippled gel P_β phase dramatically increases. The molecular origin of P_β phase formation is associated with the lipid head-group region [19]. At t_p the rotational mobility of the head-groups increases, while the acyl chains remain tightly packed. To relieve the packing frustration that arises due to changed relationship between cross-sectional areas of the head-groups and that of the acyl chains, corrugation of the membrane surface takes place. Our results indicate that GC376 induces lateral compression of the head-groups and consequent increase in stiffness of the bilayer polar region, what leads to suppression of the P_β phase formation. This suggestion is in contrast to the effect observed for baicalein, another possible SARS-CoV-2 inhibitor [31], which was found to promote formation of the P_β phase [53]. The authors suppose that intercalation of baicalein into DPPC bilayers leads to steric repulsion of the lipid head-groups, making the bilayer surface fluctuate at lower temperatures. Further, it follows that GC376 induces increase in ordering of acyl chains typical for the $L_{\beta'}$ phase. In accord with this, the main transition temperature t_m, determining the melting of lipid acyl chains, was found to increase. Due to the dominantly polar nature of GC376 molecules, it is unlikely that they penetrate deeper between the lipid acyl chains. The change in t_m, as well as the slight increase in lateral pressure detected at the C10 position of the acyl chains, may be therefore interpreted as a mediated effect, i.e. as a response to compensate changes at the polar and/or interfacial regions of the bilayer. Hereby, SAXS showed no significant influence of GC376 on the repeat distance of lipid bilayers up to GC376/DPPC = 0.01 mol/mol, neither in the gel nor in the fluid phase.

At concentrations of $0.01 < \text{GC376/DPPC} < 0.1$ mol/mol the behaviour of the system completely changes. Interaction of GC376 with head-group region of lipid bilayer leads to suppression of the pre-transition. At the same time, the bilayer repeat distance starts to increase. We suggest that increased attraction at the head-group region induced by GC376 leads to reduction of the area per lipid molecule what should be accommodated by an orthogonal expansion of lipid bilayer thickness. In the excimer fluorescence experiments reduction of the area per lipid molecule may lead to shortening of the average distance between two acyl chains in Pyr*n*PC probes. The collision frequency of the two intramolecular pyrene moieties therefore increases. As a result, we detected further increase of lateral pressures in fluid bilayers at $0.01 < \text{GC376/DPPC} < 0.1$ mol/mol (Fig. 3). At the same time, reduction of area per lipid assumes that acyl chains are in a more stretched conformation, what enhance the acyl chains packing and, in turn leads to higher gel-fluid phase transition temperatures, as we detected by DSC. Contrary to this, baicalein was found to have no significant effect on the conformation and packing of the acyl chains in DPPC bilayers [53]. The packing effect of GC376 on lipid acyl chains is obviously dominant also in the fluid phase. The increase of bilayer repeat distance (d) is even more pronounced in the fluid phase than in the gel phase lipid (Fig. 7). Similar effect was previously observed for caffeine, a small aromatic molecule, that partitions into fluid bilayers at the polar/hydrophobic

interface [20]. The authors suggest that caffeine can attract water molecules from neighbouring lipids what leads to local increase of water density at the interface. Through this mechanism, caffeine leads to an overall decrease of the gauche defect density in the membranes and an increase of membrane thickness (d_L) as resulted from experiments on a stack of oriented lipid bilayers hydrated by vapor (at relative humidity 97%). By definition, the repeat distance $d=d_L+d_W$, and our experimental approach using SAXS does not allow to resolve the contribution of the two, d_L and d_w. We assume that observed increase in d induced by GC376 might result from swelling of lamellae.

Data from both methods, DSC and SAXS show the appearance a new L_n phase at GC376/DPPC $\geq$ 0.03 mol/mol and 20 °C. It indicates an onset of domain formation and, eventually, lateral phase separation in the mixtures. We need to note, that DSC experiments were performed at significantly lower ionic strength than SAXS/WAXS experiments (see Section 2.5). Sodium ions bind tightly to the carbonyl oxygens and alter the electrostatic potential, which is largely compensated by a changed polarization of the aqueous medium and a lipid dipole orientation [4]. It is thus likely that partitioning of a charged GC376 molecule into the polar region of the lipid bilayer might be, to some extent, affected by the ionic strength of the solvent. Still, results obtained for the DPPC+GC376 system by DSC and SAXS/WAXS methods fit together very well, what suggests that the effect of ionic strength does not dominate in the studied drug-lipid interaction. Fig. 5B shows a drop in the main transition enthalpy, ΔH_m, which we attribute to disorganization of the lipid bilayer caused by phase separation. We suggest that phase separation is a response of the system to increased lateral pressures in presence of GC376. Note, that at GC376/DPPC $>$ 0.03 mol/mol we detected stabilization of lateral pressure values both in the region of C4 and C10 of the acyl chain (Fig. 3B). The L_n phase formed at CG376/DPPC $>$ 0.03 mol/mol displays further increase in t_m accompanied with an increase in ΔH_m (Fig. 5); d of the L_n phase also significantly increases (Fig. 7). These results suggest more tight packing of the lipid acyl chains in the L_n phase compared to the original L phase, leading to an increase in bilayer stiffness. Therefore, we assume that the L_n phase is enriched with GC376 molecules compared to the L phase. At the same time, the composition of the L phase seems to be conserved in entire studied concentration range (0.3 mol/mol), as deduced from the unchanged values of t_m and ΔH_m.

But, no phase separation is observed, even at highest GC376/DPPC mole ratios, in the fluid phase. SAXS diffractograms show peaks corresponding to a single lamellar phase, however with decreasing intensity and increasing width upon GC376/DPPC mole ratio (Fig. 6B). This indicates decreased ordering of stacked bilayers due to interaction with GC376. At 60 °C DPPC bilayers are fluid in a sense that there is no fixed relationship between the nearest-neighbour molecules within the interface. Dynamic processes of lipid molecules include fast motions, such as rotations around C-C bonds, rotation around molecular axis, lateral diffusion and protrusion out of the bilayer plane. This likely enables molecules of GC367 to accommodate within the bilayer without significant disruption of its structure. At the same time, a more pronounced effect of GC376 on the gel phase, compared to the fluid phase lipid, may arise from different K_P values of GC376 in the two phases. Noticeably, the K_P value determined in the present paper was obtained for the fluid phase system. The GC376 concentration in the gel phase is apparently higher than that in the fluid phase, as a consequence of $K_P^{gel} > K_P^{fluid}$. It would suggest a non-ideal mixing between GC376 and phospholipids, as observed previously for e.g. long alkanols [17]. To account for differences in partitioning of GC376 into DOPC and DPPC bilayers, respectively, we have to remind that the polar region of the two lipids is equal. Since GC376 is suggested to partition preferentially into the polar region of the bilayer, no significant difference in partitioning is assumed for the two lipid systems studied.

To sum up, obtained results imply a possibility of application of temperature-responsive lipid-based delivery systems for GC376 with sustained-release, thanks to stabilizing effect of the drug on the gel phase bilayer. Low K_P value and slight GC376 concentration dependence on vesicle size predict good bioavailability of the drug in the fluid phase. On the other hand, aside of specific inhibition of 3 CL protease, an indirect effect of GC376 on CoV's replication based on non-specific interaction with lipids of the virus envelope is suggested. Observed lateral pressure changes, increase in phase transition temperature and bilayer repeat distance, as well as domain formation within the membrane plane induced by GC376 partitioning might affect the function of virus proteins embedded in the membrane of the virus envelope, that are involved in CoV's replication process.

5. Conclusion

The interaction of small molecules with lipid membranes and the knowledge of their binding site and bilayer distribution is of great pharmacological importance and represents an active field of current biophysical research. We have studied the partitioning and effect of antiviral GC376, a potential SARS-CoV-2 inhibitor, on model lipid membranes prepared from DOPC and DPPC, respectively. Partition coefficient of GC376 between DOPC and water phase represents $K_P = 46.8 \pm 18.2$. Results suggest that GC376 partitions into lipid bilayers at the level of lipid head-groups, close to the polar/hydrophobic interface. The partitioning induces increase of lateral pressures in the membrane, mainly in the interfacial region of the bilayer, suppression of rippled P_β phase and tighter packing of lipid acyl chains. As a response, formation of domains with different GC376/DPPC composition and resulting phase separation is suggested to take place within the bilayer. These results may help to understand pharmacokinetic properties of GC376 that are inevitable for determination of drug bioavailability. Moreover, they may be useful in developing potent new antivirals targeted to inhibition of CoV's replication.

CRediT authorship contribution statement

Mária Klacsová: Conceptualization, Investigation, Formal analysis, Writing – original draft, Writing – review & editing. **Adriána Čelková:** Investigation, Formal analysis. **Alexander Búcsi:** Supervision, Formal analysis. **Juan Carlos Martínez:** Software, Writing - original draft. **Daniela Uhríková:** Funding acquisition, Conceptualization, Supervision, Writing – original draft, Writing – review & editing.

Declaration of Competing Interest

The authors declare that they have no known competing financial interests or personal relationships that could have appeared to influence the work reported in this paper.

Data Availability

Data will be made available on request.

Acknowledgement

This work was supported by VEGA 1/0223/20; APVV-21-0108; APVV 17-0250 and PP-COVID-20-0010 grant projects. SAXS/WAXS experiments were performed at BL11-NCD beamline (proposal 2021025016) at Alba Synchrotron with the collaboration of Alba staff. The authors thank ALBA staff for their helpfulness.

Appendix A. Supporting information

Supplementary data associated with this article can be found in the online version at doi:10.1016/j.colsurfb.2022.112918.

References

[1] A.O. Adedeji, S.G. Sarafianos, Antiviral drugs specific for coronaviruses in preclinical development, Curr. Opin. Virol. 8 (2014) 45–53, https://doi.org/10.1016/j.coviro.2014.06.002.

[2] Anton-Paar. (2021). The principles of dynamic light scattering. ⟨Https://Wiki.Anton-Paar.Com/En/the-Principles-of-Dynamic-Light-Scattering/⟩.

[3] G. Bains, A.B. Patel, V. Narayanaswami, Pyrene: a probe to study protein conformation and conformational changes, Molecules 16 (2011) 7909–7935, https://doi.org/10.3390/molecules16097909.

[4] R.A. Böckmann, A. Hac, T. Heimburg, H. Grubmüller, Effect of sodium chloride on a lipid bilayer, Biophys. J. 85 (3) (2003) 1647–1655, https://doi.org/10.1016/S0006-3495(03)74594-9.

[5] R.S. Cantor, Lateral pressures in cell membranes: A mechanism for modulation of protein function, J. Phys. Chem. B 101 (1997) 1723–1725, https://doi.org/10.1021/jp963911x.

[6] Y. Chen, Q. Liu, D. Guo, Emerging coronaviruses: Genome structure, replication, and pathogenesis, J. Med. Virol. 92 (4) (2020) 418–423, https://doi.org/10.1002/jmv.25681.

[7] S.J. Cowsley, R.H. Templer, D.R. Klug, Dipyrenylphosphatidylcholine as a probe of bilayer pressures, J. Fluoresc. 3 (3) (1993) 149–152, https://doi.org/10.1007/BF00862733.

[8] Y. Deng, A. Angelova, Coronavirus-induced host cubic membranes and lipid-related antiviral therapies: a focus on bioactive plasmalogens, Front. Cell Dev. Biol. 9 (2021), 630242, https://doi.org/10.3389/fcell.2021.630242.

[9] J. Drazenovic, H. Wang, K. Roth, J. Zhang, S. Ahmed, Y. Chen, G. Bothun, S. L. Wunder, Effect of lamellarity and size on calorimetric phase transitions in single component phosphatidylcholine vesicles, Biochim. Et. Biophys. Acta (BBA) - Biomembr. 1848 (2) (2015) 532–543, https://doi.org/10.1016/j.bbamem.2014.10.003.

[10] V. Frecer, S. Miertus, Antiviral agents against COVID-19: Structure-based design of specific peptidomimetic inhibitors of SARS-CoV-2 main protease, RSC Adv. 10 (66) (2020) 40244–40263, https://doi.org/10.1039/d0ra08304f.

[11] E. Glaab, G.B. Manoharan, D. Abankwa, Pharmacophore model for SARS-CoV-2 $3CL^{pro}$ small-molecule inhibitors and in vitro experimental validation of computationally screened inhibitors, J. Chem. Inf. Model. 61 (8) (2021) 4082–4096, https://doi.org/10.1021/acs.jcim.1c00258.

[12] M. Hammel, D. Uhríková, P. Balgavý, Partition of local anesthetic heptacaine homologs between phosphatidylcholine bilayers in unilamellar liposomes and aqueous phase: UV–VIS spectrophotometry study, Die Pharm. 57 (7) (2002) 499. ISSN 00317144.

[13] T. Heimburg, Thermal Biophysics of Membranes, Wiley, 2007, https://doi.org/10.1002/9783527611591.

[14] T.C. Huang, H. Toraya, T.N. Blanton, Y. Wu, X-ray powder diffraction analysis of silver behenate, a possible low-angle diffraction standard, J. Appl. Crystallogr. 26 (2) (1993) 180–184, https://doi.org/10.1107/S0021889892009762.

[15] Y. Hu, C. Ma, T. Szeto, B. Hurst, B. Tarbet, J. Wang, Boceprevir, calpain Inhibitors II and XII, and GC-376 have broad-spectrum antiviral activity against coronaviruses, ACS Infect. Dis. 7 (3) (2021) 586–597, https://doi.org/10.1021/acsinfecdis.0c00761.

[16] S. Iketani, F. Forouhar, H. Liu, S.J. Hong, F.Y. Lin, M.S. Nair, A. Zask, Y. Huang, L. Xing, B.R. Stockwell, A. Chavez, D.D. Ho, Lead compounds for the development of SARS-CoV-2 3CL protease inhibitors, Nat. Commun. 12 (1) (2021) 2016, https://doi.org/10.1038/s41467-021-22362-2.

[17] N. Janes, J.W. Hsu, E. Rubin, T.F. Taraschi, Nature of alcohol and anesthetic action on cooperative membrane equilibria, Biochemistry 31 (39) (1992) 9467–9472, https://doi.org/10.1021/bi00154a020.

[18] M.Ø. Jensen, O.G. Mouritsen, Lipids do influence protein function—the hydrophobic matching hypothesis revisited, Biochim. Et Biophys. Acta (BBA) - Biomembr. 1666 (1–2) (2004) 205–226, https://doi.org/10.1016/j.bbamem.2004.06.009.

[19] T. Kaasgaard, C. Leidy, J.H. Crowe, O.G. Mouritsen, K. Jørgensen, Temperature-controlled structure and kinetics of ripple phases in one- and two-component supported lipid bilayers, Biophys. J. 85 (1) (2003) 350–360, https://doi.org/10.1016/S0006-3495(03)74479-8.

[20] A. Khondker, A. Dhaliwal, R.J. Alsop, J. Tang, M. Backholm, A.-C. Shi, M. C. Rheinstädter, Partitioning of caffeine in lipid bilayers reduces membrane fluidity and increases membrane thickness, Phys. Chem. Chem. Phys. 19 (10) (2017) 7101–7111, https://doi.org/10.1039/C6CP08104E.

[21] J. Kieffer, J.P. Wright, PyFAI: a python library for high performance azimuthal integration on GPU, Powder Diffr. 28 (S2) (2013) 339–350, https://doi.org/10.1017/S0885715613000924.

[22] Y. Kim, S. Lovell, K.-C. Tiew, S.R. Mandadapu, K.R. Alliston, K.P. Battaile, W. C. Groutas, K.-O. Chang, Broad-spectrum antivirals against 3C or 3C-like proteases of picornaviruses, noroviruses, and coronaviruses, J. Virol. 86 (21) (2012) 11754–11762, https://doi.org/10.1128/jvi.01348-12.

[23] Y. Kim, V. Shivanna, S. Narayanan, A.M. Prior, S. Weerasekara, D.H. Hua, A.C. G. Kankanamalage, W.C. Groutas, K.-O. Chang, Broad-spectrum inhibitors against 3C-like proteases of feline coronaviruses and feline caliciviruses, J. Virol. 89 (9) (2015) 4942–4950, https://doi.org/10.1128/JVI.03688-14.

[24] N. Kučerka, J. Gallová, D. Uhríková, The membrane structure and function affected by water, Chem. Phys. Lipids 221 (2019) 140–144, https://doi.org/10.1016/j.chemphyslip.2019.04.002.

[25] H.C. Kwan, S.Y. Chen, P. Butko, B. Wieb Van Der Meer, P. Somerharju, Intramolecular excimer formation of pyrene-labeled lipids in lamellar and inverted hexagonal phases of lipid mixtures containing unsaturated phosphatidylethanolamine, Biophys. Chem. 39 (2) (1991) 137–144, https://doi.org/10.1016/0301-4622(91)85015-I.

[26] Lankalapalli, S., & Tenneti, V.S.V.K. (2022). Drug delivery through liposomes. In: Smart Drug Delivery, 1–24, eds. Ahmad, U., Haider, F., & Akhtar, J. IntechOpen. https://doi.org/10.5772/intechopen.97727.

[27] A.G. Lee, Annular events: lipid-protein interactions, Trends Biochem. Sci. 2 (10) (1977) 231–233, https://doi.org/10.1016/0968-0004(77)90117-7.

[28] N.P. Lenzo, I. Martins, B.C. Mortimer, T.G. Redgrave, Effects of phospholipid composition on the metabolism of triacylglycerol, cholesteryl ester and phosphatidylcholine from lipid emulsions injected intravenously in rats, Biochim. Et Biophys. Acta (BBA) 960 (1) (1988) 111–118, https://doi.org/10.1016/0005-2760(88)90016-1.

[29] J. Li, X. Wang, T. Zhang, C. Wang, Z. Huang, X. Luo, Y. Deng, A review on phospholipids and their main applications in drug delivery systems, Asian J. Pharm. Sci. 10 (2015) 81–98, https://doi.org/10.1016/j.ajps.2014.09.004.

[30] C.A. Lipinski, F. Lombardo, B.W. Dominy, P.J. Feeney, Experimental and computational approaches to estimate solubility and permeability in drug discovery and development settings, Adv. Drug Deliv. Rev. 46 (1–3) (2001) 3–26, https://doi.org/10.1016/S0169-409X(00)00129-0.

[31] H. Liu, F. Ye, Q. Sun, H. Liang, C. Li, S. Li, R. Lu, B. Huang, W. Tan, L. Lai, *Scutellaria baicalensis* extract and baicalein inhibit replication of SARS-CoV-2 and its 3C-like protease in vitro, J. Enzym. Inhib. Med. Chem. 36 (1) (2021) 497–503, https://doi.org/10.1080/14756366.2021.1873977.

[32] R.C. MacDonald, R.I. MacDonald, B.Ph.M. Menco, K. Takeshita, N.K. Subbarao, L. Hu, Small-volume extrusion apparatus for preparation of large, unilamellar vesicles, Biochim. Et Biophys. Acta (BBA) - Biomembr. 1061 (2) (1991) 297–303, https://doi.org/10.1016/0005-2736(91)90295-J.

[33] C. Ma, M.D. Sacco, B. Hurst, J.A. Townsend, Y. Hu, T. Szeto, X. Zhang, B. Tarbet, M.T. Marty, Y. Chen, J. Wang, Boceprevir, GC-376, and calpain inhibitors II, XII inhibit SARS-CoV-2 viral replication by targeting the viral main protease, Cell Res. 30 (8) (2020) 678–692, https://doi.org/10.1038/s41422-020-0356-z.

[34] D. Marsh, Lateral order in gel, subgel and crystalline phases of lipid membranes: Wide-angle X-ray scattering, Chem. Phys. Lipids 165 (1) (2012) 59–76, https://doi.org/10.1016/j.chemphyslip.2011.11.001.

[35] D. Marsh, *ISBN 9781420088328*. Handbook of Lipid Bilayers: Vol, 2nd ed., CRC Press, USA, 2013 https://doi.org/10.1201/b11712.

[36] V.J. Munster, F. Feldmann, B.N. Williamson, N. van Doremalen, L. Pérez-Pérez, J. Schulz, K. Meade-White, A. Okumura, J. Callison, B. Brumbaugh, V.A. Avanzato, R. Rosenke, P.W. Hanley, G. Saturday, D. Scott, E.R. Fischer, E. de Wit, Respiratory disease in rhesus macaques inoculated with SARS-CoV-2, Nature 585 (7824) (2020) 268–272, https://doi.org/10.1038/s41586-020-2324-7.

[37] J.F. Nagle, S. Tristram-Nagle, Structure of lipid bilayers, Biochim. Et Biophys. Acta (BBA) - Rev. Biomembr. 1469 (3) (2000) 159–195, https://doi.org/10.1016/S0304-4157(00)00016-2.

[38] A. Oszlánczi, A. Bóta, G. Czabai, E. Klumpp, Structural and calorimetrical studies of the effect of different aminoglycosides on DPPC liposomes, Colloids Surf. B Biointerfaces 69 (1) (2009) 116–121, https://doi.org/10.1016/j.colsurfb.2008.11.010.

[39] C. Peetla, A. Stine, V. Labhasetwar, Biophysical interactions with model lipid membranes: Applications in drug discovery and drug delivery, Mol. Pharm. 6 (5) (2009) 1264–1276, https://doi.org/10.1021/mp9000662.

[40] N.C. Santos, M. Prieto, M.A.R.B. Castanho, Quantifying molecular partition into model systems of biomembranes: an emphasis on optical spectroscopic methods, Biochim. Et Biophys. Acta (BBA) - Biomembr. 1612 (2) (2003) 123–135, https://doi.org/10.1016/S0005-2736(03)00112-3.

[41] Z. Saud, V.J. Tyrrell, A. Zaragkoulias, M.B. Protty, E. Statkute, A. Rubina, K. Bentley, D.A. White, P.D.S. Rodrigues, R.C. Murphy, H. Köfeler, W.J. Griffiths, J. Alvarez-Jarreta, R.W. Brown, R.G. Newcombe, J. Heyman, M. Pritchard, R.W. J. Mcleod, A. Arya, C.A. Lynch, D. Owens, P.V. Jenkins, N.J. Buurma, V. B. O'Donnell, D.W. Thomas, R.J. Stanton, The SARS-CoV2 envelope differs from host cells, exposes procoagulant lipids, and is disrupted in vivo by oral rinses, J. Lipid Res. 63 (6) (2022), 100208, https://doi.org/10.1016/j.jlr.2022.100208.

[42] L. Sercombe, T. Veerati, F. Moheimani, S., Y. Wu, A., K. Sood, S. Hua, Advances and challenges of liposome assisted drug delivery, Front. Pharmacol. 6 (2015) 286, https://doi.org/10.3389/fphar.2015.00286.

[43] J. Sunamoto, H. Kondo, T. Nomura, H. Okamoto, Liposomal membranes. 2. Synthesis of a novel pyrene-labeled lecithin and structural studies on liposomal bilayers, J. Am. Chem. Soc. 102 (3) (1980) 1146–1152, https://doi.org/10.1021/ja00523a035.

[44] R.H. Templer, S.J. Castle, A. Rachael Curran, G. Rumbles, D.R. Klug, Sensing isothermal changes in the lateral pressure in model membranes using di-pyrenyl phosphatidylcholine, Faraday Discuss. 111 (1999) 41–53, https://doi.org/10.1039/a806472e.

[45] D. Uhríková, A. Lengyel, M. Hanulová, S.S. Funari, P. Balgavý, The structural diversity of DNA–neutral phospholipids–divalent metal cations aggregates: a small-angle synchrotron X-ray diffraction study, Eur. Biophys. J. 36 (4–5) (2007) 363–375, https://doi.org/10.1007/s00249-006-0086-2.

[46] D. Uhríková, P. Pullmannová, M. Bastos, S.S. Funari, J. Teixeira, Interaction of short-fragmented DNA with dipalmitoylphosphatidylcholine bilayers in presence of zinc, Gen. Physiol. Biophys. 28 (2) (2009) 146–159, https://doi.org/10.4149/gpb_2009_02_146.

[47] D. Uhríková, P. Rybár, T. Hianik, P. Balgavý, Component volumes of unsaturated phosphatidylcholines in fluid bilayers: a densitometric study, Chem. Phys. Lipids 145 (2) (2007) 97–105, https://doi.org/10.1016/j.chemphyslip.2006.11.004.

[48] W.H.J. Vaes, E. Urrestarazu Ramos, C. Hamwijk, I. van Holsteijn, B.J. Blaauboer, W. Seinen, H.J.M. Verhaar, J.L.M. Hermens, Solid phase microextraction as a tool

to determine membrane/water partition coefficients and bioavailable concentrations in in vitro systems, Chem. Res. Toxicol. 10 (10) (1997) 1067–1072, https://doi.org/10.1021/tx970109t.

[49] Z. Varga, B. Fehér, D. Kitka, A. Wacha, A. Bóta, S. Berényi, V. Pipich, J.-L. Fraikin, Size measurement of extracellular vesicles and synthetic liposomes: the impact of the hydration shell and the protein corona, Colloids Surf. B: Biointerfaces 192 (2020), 111053, https://doi.org/10.1016/j.colsurfb.2020.111053.

[50] M. Vauhkonen, M. Sassaroli, P. Somerharju, J. Eisinger, Dipyrenylphosphatidylcholines as membrane fluidity probes. Relationship between intramolecular and intermolecular excimer formation rates, Biophys. J. 57 (2) (1990) 291–300, https://doi.org/10.1016/S0006-3495(90)82531-5.

[51] W. Vuong, C. Fischer, M.B. Khan, M.J. van Belkum, T. Lamer, K.D. Willoughby, J. Lu, E. Arutyunova, M.A. Joyce, H.A. Saffran, J.A. Shields, H.S. Young, J. A. Nieman, D.L. Tyrrell, M.J. Lemieux, J.C. Vederas, Improved SARS-CoV-2 M^{pro} inhibitors based on feline antiviral drug GC376: structural enhancements, increased solubility, and micellar studies, Eur. J. Med. Chem. 222 (2021), 113584, https://doi.org/10.1016/j.ejmech.2021.113584.

[52] W. Vuong, M.B. Khan, C. Fischer, E. Arutyunova, T. Lamer, J. Shields, H.A. Saffran, R.T. McKay, M.J. van Belkum, M.A. Joyce, H.S. Young, D.L. Tyrrell, J.C. Vederas, M.J. Lemieux, Feline coronavirus drug inhibits the main protease of SARS-CoV-2 and blocks virus replication, Nat. Commun. 11 (1) (2020) 4282, https://doi.org/10.1038/s41467-020-18096-2.

[53] T.-T. Wei, B.-B. Cao, X.-L. Hao, J.-Y. Gu, R.-G. Wu, The interaction of baicalein with dipalmitoylphosphatidylcholine liposomes: differential scanning calorimetry, synchrotron X-ray diffraction, and fourier transform infrared studies, Thermochim. Acta 703 (2021), 178993, https://doi.org/10.1016/j.tca.2021.178993.

[54] H. Xu, F. Ye, M. Hu, P. Yin, W. Zhang, Y. Li, X. Yu, Y. Deng, Influence of phospholipid types and animal models on the accelerated blood clearance phenomenon of PEGylated liposomes upon repeated injection, Drug Deliv. 22 (5) (2014) 598–607, https://doi.org/10.3109/10717544.2014.885998.

[55] K.S. Yadav, D.K. Mishra, A. Deshpande, A.M. Pethe, Levels of drug targeting, 269–305, ed. Tekade, R.. Basic Fundamentals of Drug Delivery, Elsevier, 2019, https://doi.org/10.1016/B978-0-12-817909-3.00007-8.

[56] H. Yang, W. Xie, X. Xue, K. Yang, J. Ma, W. Liang, Q. Zhao, Z. Zhou, D. Pei, J. Ziebuhr, R. Hilgenfeld, K.Y. Yuen, L. Wong, G. Gao, S. Chen, Z. Chen, D. Ma, M. Bartlam, Z. Rao, Design of wide-spectrum inhibitors targeting coronavirus main proteases, PLoS Biol. 3 (10) (2005), e324, https://doi.org/10.1371/journal.pbio.0030324.